PERGAMON

Journal of Structural Geology 24 (2002) 277–287

JOURNAL OF STRUCTURAL GEOLOGY

www.elsevier.com/locate/jstrugeo

Mechanical models of trishear-like folds

Kaj M. Johnson*, Arvid M. Johnson

G.K. Gilbert Geomechanics Laboratory, Purdue University, Earth and Atmospheric Sciences, 1397 CIVL, West Lafayette, IN 47907, USA

Received 10 August 2000; accepted 13 March 2001

Abstract

Previous workers have formulated velocity descriptions of the trishear kinematic model of fault propagation-folds, which are inherently non-unique. We present two complete mechanical models of fault-related folding and assess the validity of the assumptions used in the assignment of velocities in the trishear description and to eliminate the untenable situation of an infinite number of possible solutions for velocity fields. The mechanical model of forced-folding, *Forced Fold,* based on viscous folding theory, is used to derive the velocity fields in an anisotropic sedimentary cover overlying faulted and displaced rigid basement blocks. The solution of displacements around a stress-free fault in an elastic body is used to model fault-arrest folds that form around a fault imbedded in a deformed medium. The results indicate that the velocity fields assumed in the trishear model more closely resemble the velocities derived in the mechanical *Forced Fold* model than the mechanical model of fault-arrest folding. The *Forced Fold* model produces a triangular region of concentrated deformation similar to the trishear region assumed in the kinematic models, while the deformation produced by the fault-arrest model is not concentrated within a triangular zone.

Keywords: Mechanical models; Trishear folds; Velocity fields

1. Introduction

In the last decade, structural geologists have devised various kinematic models of forced-folds and fault-propagation folds to reproduce the geometry of basement-involved uplifts of the Rocky Mountain foreland (Erslev, 1991; Narr and Suppe, 1994; Hardy and Ford, 1997; Allmendinger, 1998; Mitra and Mount, 1998). The curviplanar, trishear velocity model (Fig. 1A) was introduced by Erslev (1991) to replicate the geometry of fault-propagation folds more nearly accurately than the parallel kink-like (Fig. 1B) graphical constructions by, for example, Suppe (1985) and Narr and Suppe (1994). More recently, Hardy and Ford (1997) and Zehnder and Allmendinger (2000) have produced velocity models that are variations on the original method proposed by Erslev (1991). The velocity methods create fold forms by specifying velocities at points in the medium surrounding the fold-producing fault. The velocities are assigned according to a set of rules that assume area balance within a triangular shear zone.

Although many authors have compared fold forms generated with the trishear method with fold forms in experiments and in the field, the validity of the assumed trishear velocity distributions has not been checked with results derived from theoretical models of fault-related folding. The need for such theoretical models was recognized by Zehnder and Allmendinger (2000), who showed that one can generate an infinite number of velocity distributions that satisfy the conditions considered in the kinematic models of Erslev (1991) and Hardy and Ford (1997).

In this paper we present two mechanical models of fault-related folding and compare the velocities and displacements produced by the theoretical analyses with the velocity fields assumed in the trishear kinematic model.

2. Velocity fields and fold forms according to trishear kinematic model

2.1. General conditions

The essential elements of the trishear velocity models consist of three regions in the vicinity of a fault tip in which different velocity fields are assigned (Fig. 2A). Constant velocity fields are assigned in regions I and II. The material in region I, above the fault, moves as a rigid body in the x-direction, parallel to the fault. The material in region II, below the fault, is also rigid but does not move. Since the materials in rigid regions I and II move relative to one another, the material in the triangular, 'trishear' zone

* Corresponding author. Now at: Geophysics Department, Stanford University, Stanford, CA, USA.

E-mail address: kaj@pangea.stanford.edu (K.M. Johnson).

0191-8141/01/$ - see front matter
PII: S0191-8141(01)00062-1

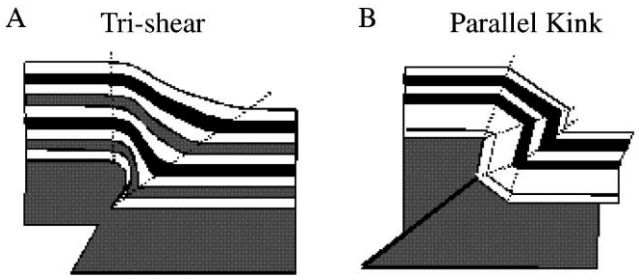

Fig. 1. Kinematic models of fault-related folds. (A) Trishear fold (Erslev, 1991). (B) Fault-propagation fold (Narr and Suppe, 1994).

(zone III in Fig. 1A), must deform. The resulting fold form is computed at multiple time steps by integrating the velocities at points defining passive markers within the trishear zone.

In order to describe how the material within the trishear zone moves, it is assumed:

1. The material does not change volume. Zehnder and Allmendinger (2000) explicitly assume that the two-dimensional continuity equation,

$$\frac{\partial v_x}{\partial v} + \frac{\partial v_y}{\partial y} = 0$$

2. applies, and implicitly assume plane flow, that is the velocity in the z-direction is zero. Application of the continuity equation guarantees that cross-sectional area is preserved (if density remains constant), which is a sufficient condition for balanced structural profiles.
3. The velocity normal to the fault is zero along the boundary between regions I and III and the velocity parallel to the fault is equal to the velocity parallel to the fault throughout region I. Thus one boundary condition is

$$v_x = v_0,\ v_y = v_0 \text{ at } y = x\tan\varphi_1$$

4. The material within trishear region III is welded to the rigid material in region II so that a second boundary condition is that, along the boundary between regions II and III

$$v_x = v_y = v_0 \text{ at } y = -x\tan\varphi_2$$

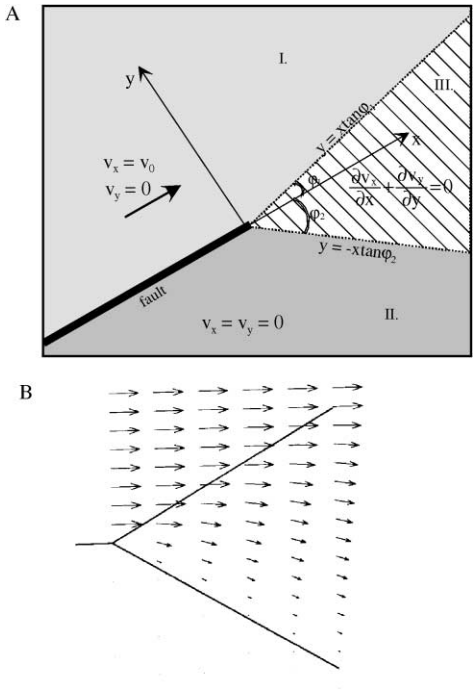

Fig. 2. (A) The geometry assumed in trishear. Velocities are uniform and parallel to the fault in region I and zero in region II. A velocity distribution satisfying continuity and boundary conditions is assigned in region III. (B) An example of a trishear velocity field derived by Zehnder and Allmendinger (2000) for the case $\vartheta_1 = \vartheta_2 = 15°$.

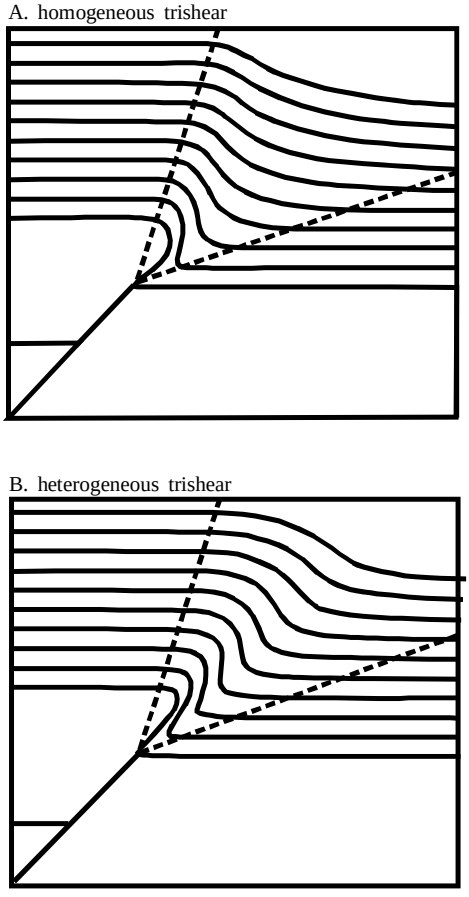

Fig. 3. Two types of trishear (after Erslev, 1991). (A) Homogeneous trishear. (B) Heterogeneous trishear.

Therefore, the parameters that can be varied are ϑ_1 and ϑ_2, v_0, and the velocity distribution, v_x and v_y, within the trishear zone. The fault tip may also be extended into the triangular region to represent fault-propagation folds, thus the propagation to slip ratio may also be specified. Although authors vary these parameters when attempting to reproduce the geometry of folds, only one of the parameters is clear: v_0 is a rigid-body motion. It is quite unclear what physical,

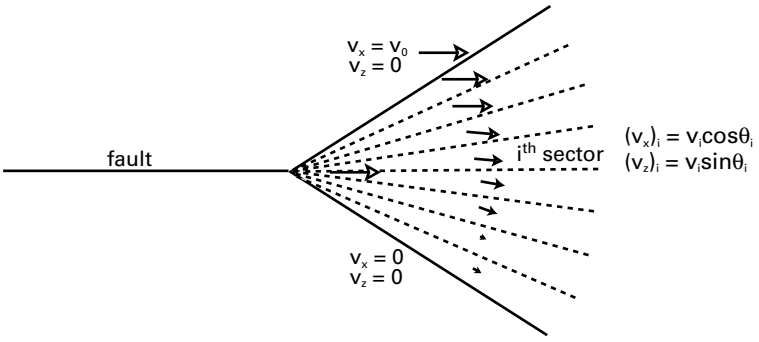

Fig. 4. The trishear velocity field devised by Hardy and Ford (1997).

mechanical conditions the parameters ϑ_1 and ϑ_2 or the velocity distribution, v_x and v_y, describe (Allmendinger, 1998).

2.2. Erslev kinematic model

Erslev (1991) devised two types of trishear deformation, which he called homogeneous and heterogeneous trishear. Fig. 3 displays the fold forms of both types. In his constructions, line segments perpendicular to the fault, called tie lines, are constructed in the triangular region. Homogeneous trishear rotates the tie lines uniformly throughout deformation, whereas in heterogeneous trishear, segments of tie lines in the center of the triangular zone rotate more than those near the triangle boundaries. Examples of both types of folds are shown in Fig. 3. These folds were generated with a 45° reverse fault and $\vartheta_1 = \vartheta_2 = 30°$.

2.3. Hardy/Ford kinematic model

Hardy and Ford (1997) divided the triangular trishear region (III, Fig. 2A) into sectors and satisfied continuity in each sector (Fig. 4). They assumed that the magnitude of the velocity within each sector was constant, but the sector velocities decreased linearly from the top of the triangular region to the bottom. The components of velocity in the *i*th sector are given by the expressions

$$(v_x)_i = v_i\cos(\theta_i) \tag{1a}$$

$$\left(v_y\right)_i = v_i\sin(\theta_i) \tag{1b}$$

where v_i is the net velocity in the *i*th sector and θ_i is direction of the velocity vector, determined by solving Eqs. (1a) and (1b), together with the so-called block contact condition

$$\left(v_y\right)_i - (v_x)_i\,\partial f/\partial x = \left(v_y\right)_{i+1} - (v_x)_{i+1}\,\partial f/\partial x \tag{2}$$

where f is the boundary. The expressions for the velocity components (Eqs. (1a) and (1b)) satisfy continuity.

2.4. Zehnder/Allmendinger kinematic model

Zehnder and Allmendinger (2000) investigated more thoroughly the velocity description of trishear. They presented a general method to derive solutions to the continuity equation that satisfy the boundary conditions. Fig. 2B is one of their velocity field solutions, which satisfies the three sets of conditions outlined above. As one follows a row of grid points, such as that immediately above the fault tip, one sees that the vectors decrease in length and turn downward more with increasing horizontal distance from the fault tip. As one follows a column of grid points, one sees that the vectors decrease more rapidly in length and turn downward more with increasing depth.

The analysis by Zehnder and Allmendinger (2000) presents a dilemma, though. How does one select a solution? They show that there is in fact an infinite number of possible velocity formulations that satisfy the three conditions outlined above. This result illustrates a weakness of the trishear kinematic model (indeed, of any strictly kinematic description of a process): in kinematic descriptions there is an infinite number of ways to assign motions that satisfy the condition of continuity (area conservation). Many of these motions are physically untenable. Thus it is clear that other conditions, in addition to continuity, must be satisfied to describe the geometry of fault-related folds (or any other physical process).

3. Velocity fields and fold forms according to forced-fold mechanical model

It is well known in continuum mechanics (e.g. Love, 1944; Timoshenko and Gooder, 1951; Malvern, 1969; Johnson, 1970, 1977; Johnson and Fletcher, 1994; Fletcher and Pollard, 1999) that properly formulated mechanical models of processes, such as fault-related folding, include these other conditions. The solutions provide the velocity field uniquely for a given set of conditions. A complete mechanical model contains several basic equations: constitutive relations, compatibility of strains (elastic body) or of deformation rates (viscous body), equilibrium equations, and sufficient traction and velocity boundary conditions, all of which are necessary to determine the displacement (or velocity) and stress fields in the deforming medium. In some

cases, other equations, such as the continuity equations, are also invoked depending on the types of processes being modeled.

We will consider mechanical models of two very different mechanisms of fault-related folding. The first is a solution derived by Johnson and Johnson (2001) and Patton and Fletcher (1998a,b) that uses modern viscous folding theory (Johnson and Fletcher, 1994) to model forced-folds. The second uses the solution given by Tada et al. (1985) for the displacements around a crack imbedded in an infinite elastic body subjected to far-field stresses.

In this paper we use the term forced-fold for folds that form by a specific mechanism. The forced-folding mechanism consists of a single or multi-layer (sedimentary cover) that deforms more or less passively over rigid basement blocks that are displaced along planar or listric faults (Stearns, 1978).

3.1. Solution of boundary-value problem

All of the following equations are required in order to derive a solution for problems of forced folding of a viscous anisotropic fluid. For plane flow (zero flow in the *y*-direction) the *constitutive equations* are given by Eqs. (8.2.7) in Johnson and Fletcher (1994, p. 373)

$$\sigma_{XX} = 2\mu_n D_{XX} - p \tag{3a}$$

$$\sigma_{ZZ} = 2\mu_n D_{ZZ} - p \tag{3b}$$

$$\sigma_{XZ=2}\mu_{sD_{XZ}} \tag{3c}$$

in which μ_n is the normal and μ_s is the shear coefficient of viscosity, p is the mean pressure, σ is stress and D is deformation rate

$$D_{XX} = (\partial v_X/\partial x) \tag{4a}$$

$$D_{ZZ} = (\partial v_Z/\partial z) \tag{4b}$$

$$D_{XZ} = (1/2)[(\partial v_X/\partial z) + (\partial v_Z/\partial x)] \tag{4c}$$

The condition of *no volume change* is that

$$D_{XX} + D_{ZZ} = (\partial v_Z/\partial z) + (\partial v_X/\partial x) = 0 \tag{5}$$

The *equations of force and moment equilibrium*, combined with the constitutive equations, give differential equations of the form of Eqs. (8.3.3) in Johnson and Fletcher (1994, p. 374)

$$(2\mu_n - \mu_s)\left(\partial^2 v_X/\partial x^2\right) + \mu_s\left(\partial^2 v_X/\partial z^2\right) = (\partial P/\partial x) \tag{6a}$$

$$(2\mu_n - \mu_s)\left(\partial^2 v_Z/\partial z^2\right) + \mu_s\left(\partial^2 v_Z/\partial x^2\right) = (\partial P/\partial z) \tag{6b}$$

Introducing a stream function, ψ, such that (Eqs. (8.3.3) in Johnson and Fletcher (1994, p. 374))

$$v_X = -(\partial\psi/\partial z) \tag{7a}$$

$$v_Z = -(\partial\psi/\partial x) \tag{7b}$$

we have the general, fourth-order differential equation that needs to be solved (Eqs. (8.3.4) in Johnson and Fletcher (1994, p. 375))

$$\frac{\partial^4\psi}{\partial x^4} + 2\left(2\frac{\mu_n}{\mu_s} - 1\right)\frac{\partial^4\psi}{\partial x^2\partial z^2} + \frac{\partial^4\psi}{\partial z^4} = 0 \tag{8}$$

The relevant solution to the velocities in the mechanical model has the form

$$v_x = \sum_{m=1}^{\infty} -\left[a_m g_1 e^{g_1 m/z} - b_m g_1 e^{-g_1 m/z} + c_m g_2 e^{g_2 m/z} - d_m g_2 e^{g_2 m/z}\right] e^{imlx} \tag{9a}$$

$$v_z = \sum_{m=1}^{\infty} -i\left[a_m g_1 e^{g_1 m/z} - b_m g_1 e^{-g_1 m/z} + c_m g_2 e^{g_2 m/z} - d_m g_2 e^{g_2 m/z}\right] e^{imlx} \tag{9b}$$

$$g_{1,2} = \sqrt{2\frac{\mu_n}{\mu_s} - 1 \pm \sqrt{\left(2\frac{\mu_n}{\mu_s} - 1\right)^2 - 1}} \tag{9c}$$

where the complex coefficients a_m, b_m, c_m, and d_m are determined by the boundary conditions and $l = 2\pi/L$ where L is the wavelength of the surface at the basement/cover contact. We solve for the mean pressure by substituting Eqs. (9a)–(9c) into Eqs. (6a) and (6b) and integrating. Then we solve for the stresses by substituting the resulting expression for mean pressure and Eqs. (9a)–(9c) into the constitutive equations (3a)–(3c). Thus we have the complete solution, for velocities and stresses, throughout the body, to within values given by the boundary conditions. Note that we did not have to guess anything. The velocities and stresses come from the solution. All that remains is to evaluate the arbitrary constants in terms of the boundary conditions.

As discussed in Johnson and Johnson (2001) and Patton and Fletcher (1998a,b), a velocity boundary condition is applied at the basement-cover contact, determined from the rigid motion of basement blocks along a fault, and a traction-free boundary condition on the upper ground surface (The normal and shear tractions remain zero on the ground surface.) We have set up the solution so that we can study effects of several variables:

1. Shape of the fault. The fault may be a plane or a circular cylindrical arc.
2. Slip on the fault. Only dip slip is allowed, but faulting may be normal or reverse.
3. Anisotropy (μ_n/μ_s) of the cover. The anisotropy ratio is the ratio of the coefficient of viscosity in layer-parallel and layer-normal shearing to the coefficient of viscosity in layer-parallel and layer-normal compression. Each value of anisotropy (μ_n/μ_s) models certain rock

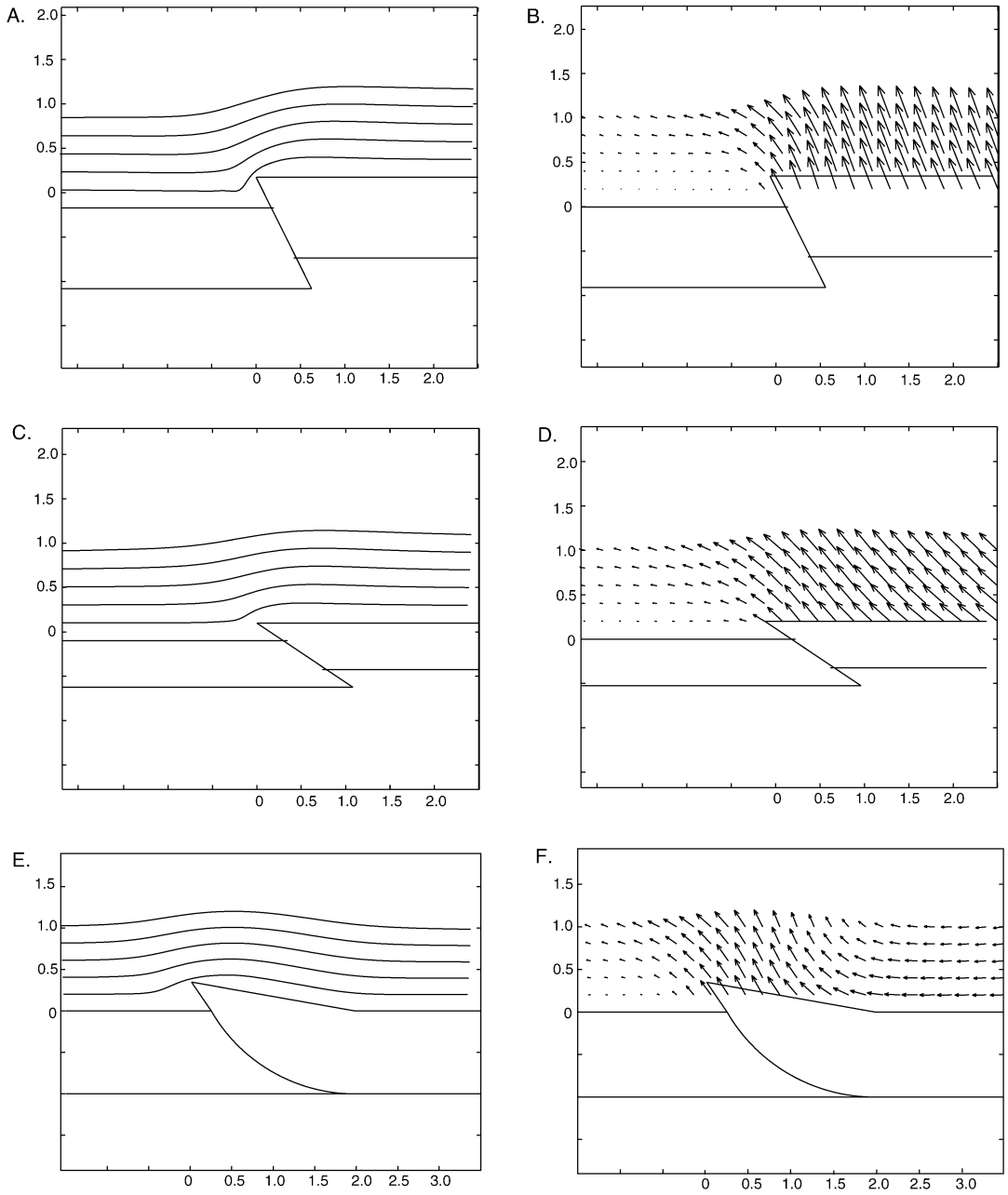

Fig. 5. Effect of shape and dip of basement fault on fold forms and velocities in sedimentary cover. Fold forms and velocities calculated with the Forced-Fold mechanical model. Each fold is produced in an isotropic cover welded to the basement. (A and B) 60° reverse fault. (C and D) 30° thrust fault. (E and F) Reverse listric fault.

properties. For example, a sedimentary cover composed of interbedded stiff and soft layers might have $\mu_n/\mu_s = 3$. For many thin layers slipping freely, the value would be larger.

4. Basement-cover contact. We can vary the resistance to slip along the basement/cover contact from completely detached (zero resistance to sliding) to completely welded (no slippage).

We have written and compiled a computer program in Matlab, *Forced-Fold*,[1] that implements the solution with a GUI (graphical user's interface).

3.2. Planar or listric basement fault

Fig. 5 displays fold forms and velocities generated by *Forced Fold* which models the deformation of layered

[1] A trial version of the computer program *Forced-Fold* may be downloaded from the Purdue University, Department of Earth and Atmospheric Sciences *Faux Pli Software* website: http://www.eas.purdue.edu/fauxpli/.

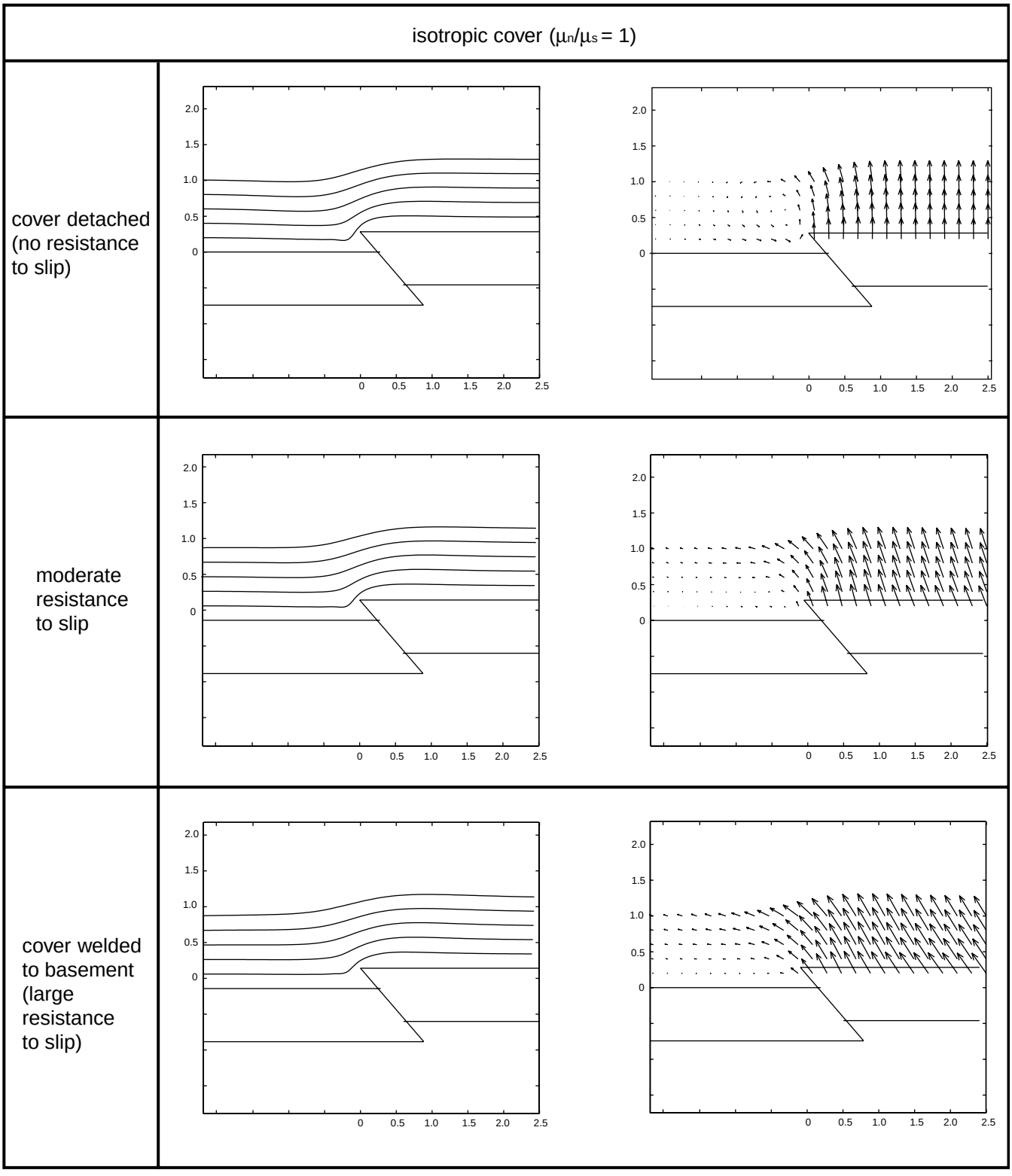

Fig. 6. Effect of anisotropy and degree of detachment from basement on fold form. Fold forms and velocities calculated with Forced-Fold mechanical model for reverse faulting. On left are solutions for isotropic cover. On right are solutions for anisotropic cover. Top row is for no resistance to slip, middle row for moderate resistance to slip, and lower row for very high resistance to slip between cover and rigid basement.

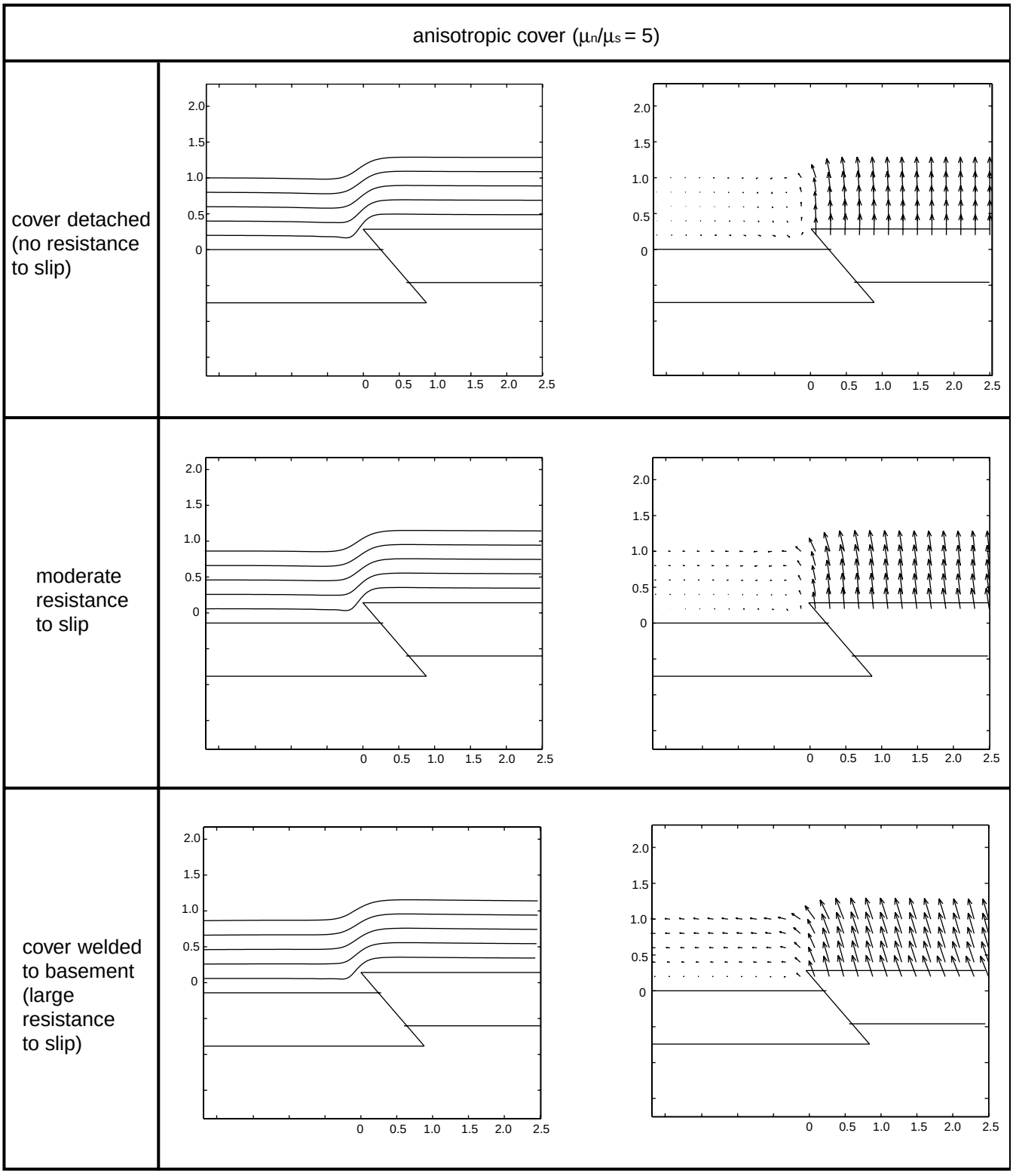

Fig. 6. (*continued*)

sedimentary cover overlying displaced, rigid basement blocks. The folds shown in Fig. 5 were formed in an isotropic (linear) cover welded to the basement with different basement-fault geometries. The footwall is fixed in each example by specifying zero velocities along the basement-cover contact on the footwall, and non-zero velocities parallel to the fault along the basement-cover contact on the hanging wall.

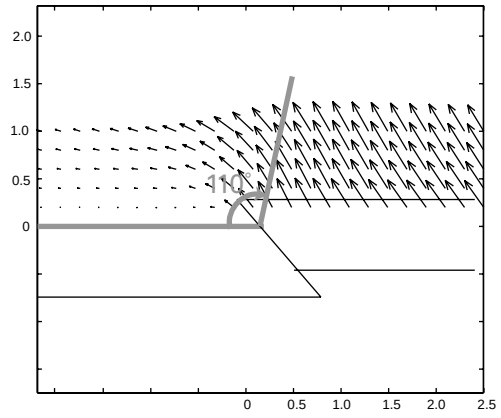

Fig. 7. Solution for velocities according to Forced-Fold with superposition of hypothetical trishear boundaries. Isotropic cover welded to basement.

In the case of planar basement faults, the velocities are nearly uniform in magnitude and direction over the hanging wall block and parallel to the fault. The velocities above the footwall block range from small horizontal velocities at the ground surface to zero at the basement-cover contact. Thus the velocity distributions show that for planar basement faults the velocities follow the general pattern assumed in the trishear kinematic models (Fig. 5B and D) but not for listric faults (Fig. 5F).

The overall shapes of the folds are roughly monoclinal for the planar faults and asymmetric/anticlinal for the listric fault. The monoclinal fold is narrow near the tip of the fault and broadens upward to the ground surface. For the listric fault the shape is more strongly asymmetric near the fault tip than near the surface.

The shapes of the forelimbs of the forced folds in isotropic cover are roughly the same, regardless of the geometry of the basement fault. The forelimb thickens near the synclinal hinge and thins between the anticlinal and synclinal hinges.

3.3. Anisotropy of the cover

Thus far we have explored the effect of shape and sense of slip on the basement fault on the displacement and velocity distributions. The sedimentary cover has been isotropic and has been welded to the rigid basement blocks. Now in Fig. 6 we consider only reverse slip on a 45° inclined fault and explore the effects of anisotropy of the sedimentary cover and the resistance to slip at the basement/cover contact.

It is clear that the anisotropy of the cover markedly influences the geometry of the forced-fold. The forelimb in isotropic cover increasingly widens upward from the tip of the fault where the limb dips are steeper to the top surface where the limb dips are shallower. The forelimb in the anisotropic cover is essentially of constant width and dip, from near the fault tip to the ground surface. Thus the forelimb closely resembles a kink fold with rounded hinges. The forelimbs in anisotropic cover resemble those in the parallel kink constructions (Fig. 1B). The forelimb width and dips are uniform with depth in the cover.

With the results thus far, the forced-fold theoretical model has already explained an important condition responsible for strikingly different perceptions of the shapes of forced-folds — the sharp kink-like forced folds depicted by Narr and Suppe (1994), Mitra and Mount (1998) and many others, and the rounded, more open forced folds depicted by Erslev (1991) and others. By varying the anisotropy of the sedimentary cover one can vary the shape of the forced fold, over a wide range of shapes.

3.4. Nature of basement/cover contact

The velocity distributions in the hanging wall are also affected by the degree of bonding between the sedimentary cover and the basement (Fig. 6). The bonding considered in the theoretical model ranges from complete detachment (free slip) to welding of the sedimentary cover to the basement. For both isotropic and anisotropic sedimentary cover, the degree of bonding determines the direction of displacement in the sedimentary cover over the hanging wall basement block. If detached, the sedimentary cover moves vertically, even though the faulting is reverse. If partially welded, the cover moves obliquely to the fault, and if completely welded, the sedimentary cover moves in the direction of faulting.

Fig. 6 shows that, regardless of the degree of anisotropy of the cover, much of the cover above the hanging wall block has uniform velocities. The velocities above the hanging wall block are nearly uniform and parallel to the fault surface in the cover that is welded to the basement. In addition, the velocities over the footwall block are larger in the cover welded to the basement than in the cover that is partly or totally detached from the basement.

3.5. Comparison with trishear model

We can show with the theoretical examples that the assumption of a triangular zone of deformation in trishear kinematic models is reasonable for the forced-fold mechanism under certain conditions.

The gross form of the velocity distributions of the forced-fold and the trishear kinematic description are similar. Fig. 7 shows a triangular boundary, with vertex angle of 110°, purposefully placed in the velocity distribution of the theoretical fold shown in Fig. 6 with isotropic cover welded to basement. It is clear that one can imagine a roughly triangular zone within which the velocities are changing, that is, within which deformation is concentrated. Outside of the triangular zone, above the hanging wall block, the cover behaves as a nearly rigid body; the velocities are uniformly parallel to the fault. The footwall block was assumed rigid in our model, so the velocities are zero there, as in the region below the fault in the trishear models. The velocities within this triangular region grossly resemble the velocities in the triangular region of a trishear model. As

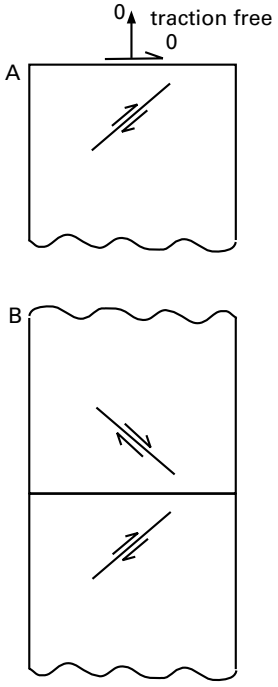

Fig. 8. Solutions for single faults superimposed to derive an approximate solution for an inclined fault near the ground surface. (A) The shear and normal tractions must be zero on the upper (ground) surface. (B) The same sense and amount of slip are applied to a fault inclined 45° and its image across the upper surface to cancel the normal and shear stresses at the upper, ground surface.

shown in Fig. 2B, the velocities in a trishear model of Zehnder and Allmendinger range from a maximum velocity at the top of the triangular zone, over the hanging wall, to zero at the bottom.

Note that in all the theoretical forced-folds with straight basement faults (Figs. 5 and 6), the trishear-like triangular region of localized deformation falls within a triangle with vertex angle of ~110° (one wall of the triangle lies along the basement/cover contact in the footwall and the other wall lies in the hanging wall side). Although the vertex angle is a parameter that is free to be varied in the trishear model, it is unclear, as pointed out by Allmendinger (1998), what physical property would control such a parameter. Our theoretical results suggest that the appropriate vertex angle for forced-folds is about 110°, although other mechanisms of fault-related folding may produce different results. While the vertex angle is uniformly ~110°, the theoretical examples show that the velocity distributions within the triangular zone depend on all of the parameters we have chosen to vary: the dip of the fault (Fig. 5B and D), the degree of detachment between basement and cover (Fig. 6), and the anisotropy of the cover (Fig. 6).

The trishear assumption about the movement of the hanging wall block fails if the cover is not perfectly welded to the basement. It is assumed in the trishear model that the velocities outside of the triangular region, above the hanging wall, are uniform and parallel to the fault surface. We show in Fig. 6 that this is the case in the mechanical model only when the cover is welded to the basement. When the cover is not completely welded to the basement, there is a discontinuity in velocity at the basement-cover contact. Furthermore, the trishear assumption about a triangular shear zone is not valid for forced-folds produced by curved basement faults (Fig. 5F).

4. Fold form for fault-arrest mechanical model

In the previous sections of this paper we have compared the geometry and kinematics of the trishear construction with the geometry and kinematics of the forced-fold theoretical model. The trishear geometry appears to be best modeled in terms of an isotropic or anisotropic cover welded to the basement. In the forced-fold model, however, the deformation occurs within non-faulted cover rocks overlying displaced rigid basement blocks. The trishear model is used to describe the deformation near the tip of a fault that has propagated into the deformed medium. Thus we are motivated to compare the trishear construction to fold forms produced near the tip of a fault within the deformed medium. We use a very simple model of fault-arrest folding consisting of a stress-free crack near a free surface in an elastic medium.

4.1. Solution of boundary-value problem

We use the solution of Tada et al. (1985) to calculate the displacements around the tip of an inclined, two-dimensional fault imbedded in an incompressible, elastic medium with a traction free surface (ground surface). In this solution, the infinite elastic medium is initially loaded and then the shear stress along the imbedded crack is dropped. The fold is produced by stress drop along the fault. The displacements in an incompressible elastic material around a fault along which the shear stress drops by an amount τ_{xy} are:

$$u_x = \frac{\tau_{xy}}{2G}\left[\mathscr{I}\left\{\mathrm{eq}\sqrt{z^2 - a^2}\right\} + y\left(\mathscr{R}\left\{\frac{1}{\sqrt{1-(a/z)^2}}\right\} - 2\right)\right] \tag{10a}$$

$$u_y = \frac{\tau_{xy}}{2G}\left[y\mathscr{I}\left\{\frac{1}{\sqrt{1-(a/z)^2}}\right\}\right] \tag{10b}$$

in which $\mathscr{R}$ and $\mathscr{I}$ are real and complex parts, and z is the complex coordinate, $z = x + iy$.

We let the x-axis be vertical and the y-axis horizontal, and draw grid lines parallel to the horizontal, y-axis (Fig. 9). The horizontal lines within the elastic body are passive markers.

While this elastic solution provides displacements rather than velocities, as in the viscous solution for forced-folding, we can compare the fold forms. After integrating the velocities of the trishear kinematic description, we compare

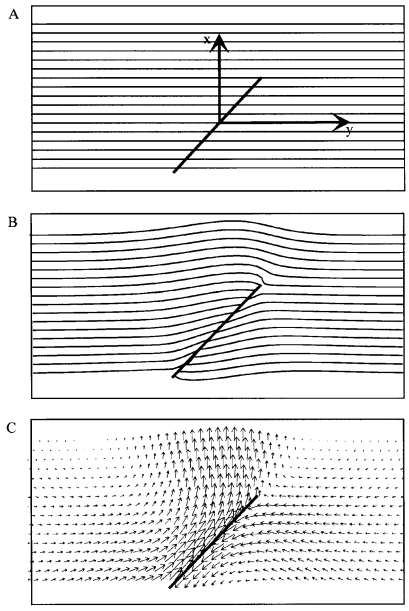

Fig. 9. (A) Geometry of the fault and passive markers in the mechanical model of a fault imbedded in an elastic medium. (B) Fold form produced by dropping the stresses on the fault in the initially loaded medium. The maximum displacement on the fault is 0.2 times the fault length. (C) Displacements in the elastic medium after the fault slips.

the displacement field of the trishear model with the displacement field of the fault in the elastic medium.

In order to derive an approximate solution for the effect of the traction-free ground surface, we superimpose solutions for two faults. The solution needs to satisfy the condition that the shear and normal tractions are zero on the upper (ground) surface. In order to model a traction free ground surface, we reflect the fault and put its center an equal distance into the reflected medium above the ground surface (Fig. 8) and apply the same sense and amount of slip on both faults. If the fault and its image are inclined at 45°, as shown in Fig. 8, the shear and normal tractions on the surface sum to zero, so the superposition solves the problem approximately. Although the approximation is satisfactory for our purposes, more nearly exact solutions can be obtained by other methods.[2]

4.2. Fold form near tip of near-surface fault

Fig. 9 shows a 45° dipping fault in an elastic medium that is initially loaded in horizontal compression. Straight horizontal markers were drawn after loading. The medium is initially loaded such that, after the stresses along the fault are dropped, and the fault slips, the maximum displacement along the fault is 0.2 times the fault length. The load is maintained, and the markers remain deformed.

The fold is a fault-arrest fold, because the fault was not allowed to propagate. It simply slipped, maintaining its length. The shape of the fold in the passive markers is an asymmetric fold (Fig. 9B). Near the ground surface the passive layers are folded nearly symmetrically. Near the fault tip the folding is nearly monoclinal, with steeply-dipping layers in the forelimb and gently-dipping layers in the rotated backlimb. The displacements around the fault are shown in Fig. 9C. Away from the fault the displacements are roughly horizontal. Closer to the fault, the displacements increase and become parallel with the fault. Uplift is generated just behind the fault tip where the displacements are largely vertical.

The forelimb geometry of the fault-arrest fold is similar to the forelimb geometry of the forced-fold (Figs. 5 and 6) in isotropic media. In each fold the forelimb dips steeply near the fault tip and dips more shallowly at the ground surface. In both models the layering is thinned in the forelimb and thickened in the anticlinal hinge. A characteristic of the fault-arrest fold that is strikingly different from the forced-folds overlying straight basement faults is the existence of backlimb rotation. The back limb dips gently and nearly uniformly to the left in the fault-arrest fold. The forced-folds overlying straight basement faults (Figs. 5 and 6) display little backlimb rotation.

The deformation in the fault-arrest fold is clearly different from trishear deformation — there is no trishear-like triangular zone of localized deformation. While the forelimb geometry resembles the forelimb geometry of trishear folds — with steeply dipping layers near the fault tip and decreasing dips towards the ground surface — the backlimb is folded. A folded backlimb cannot be generated under the assumptions of the trishear model because the velocity region within the hanging wall is assigned a constant velocity.

5. Conclusions

A complete mechanical solution, *Forced-Fold,*provides a unique solution for each set of parameters and eliminates the untenable situation of an indefinite number of possible solutions for velocity fields recognized by Zehnder and Allmendinger (2000).

We have demonstrated in this paper that the assumptions used in the trishear description — specifically, the triangular zone of deformation and the boundary conditions — are more nearly appropriate for the forced-fold mechanism than the fault-arrest fold mechanism. Based on the results of the mechanical analyses of velocities and displacements in fault-related folds, *Forced-Fold* produces uniform velocities above the hanging wall of the basement fault, much like the uniform velocity distribution assumed above the hanging wall and outside the triangular region of the trishear construction. Furthermore, in the case where the cover is welded to the basement, the velocities above the hanging wall block are parallel to the fault, as is assumed in trishear. A triangular region of concentrated deformation with a vertex angle of about 110°, similar to the trishear

[2] For example, see Pollard and Holzhausen (1979).

triangular zone, can be imagined in the forced-folds. As illustrated in Fig. 7, the lower boundary of the triangular region would lie on the footwall side of the basement-cover contact, below which the velocities are zero. The upper boundary of the triangular region would lie above the hanging wall side of the fault.

We have also compared the displacements around a fault in an elastic medium with the trishear displacements because the trishear description models fault-propagation folding. The trishear assumptions are clearly not appropriate to the problem of a fault imbedded in a deformed medium, such as the fault-arrest elastic model. The fault-arrest model produces a complicated field of displacements that is not consistent with the trishear assumptions. The backlimb of the fault-arrest fold is deformed and thus there is not a distinct triangular region of concentrated deformation around the tip of the fault, as is assumed in the trishear model.

Acknowledgements

We would like to thank the reviewers Alan Zehnder and Eric Erslev for their helpful comments. We are grateful to the Department of Energy (grant DE-FG02-98ER14886) for support of this research.

References

Allmendinger, R.W., 1998. Inverse and forward numerical modeling of trishear fault-propagation folds. Tectonics 17 (4), 640–656.

Erslev, E.A., 1991. Trishear fault-propagation folding. Geology 19, 617–620.

Fletcher, R.C., Pollard, D.D., 1999. Can we understand structural and tectonic processes and their products without appeal to a complete mechanics?. Journal of Structural Geology 21 (8–9), 1071–1088.

Hardy, S., Ford, M., 1997. Numerical modeling of trishear fault propagation folding. Tectonics 16 (5), 841–854.

Johnson, A.M., 1970. Physical Processes in Geology. Freeman, Cooper and Company, San Francisco, 577pp.

Johnson, A.M., 1977. Styles of Folding. Elsevier, New York, 406pp.

Johnson, A.M., Fletcher, R.F., 1994. Folding of Viscous Layers. Columbia University Press, New York, 461pp.

Johnson, K.M., Johnson, A.M., 2001. Volume 5: Mechanical analysis of the geometry of forced-folds. In: The Purdue Faux Pli Manual, Purdue Research Foundation, Purdue University. Available for download at www.eas.purdue.edu/fauxpli.

Love, A.E.H., 1944. A Treatise on the Mathematical Theory of Elasticity. Dover Publications, New York.

Malvern, L.E., 1969. Introduction to the Mechanics of a Continuous Medium. Prentice-Hall, Englewood Cliffs, NJ, 713pp.

Mitra, S., Mount, V.S., 1998. Foreland basement-involved structures. American Association of Petroleum Geologists 82 (1), 70–109.

Narr, W., Suppe, J., 1994. Kinematics of basement-involved compressive structures. American Journal of Science 294, 802–860.

Patton, T.L., Fletcher, R.C., 1998a. Mathematical block-motion model for deformation of a layer above a buried fault of arbitrary dip and sense of slip. Journal of Structural Geology 17 (10), 1455–1472.

Patton, T.L., Fletcher, R.C., 1998b. A rheological model for fractured rock. Journal of Structural Geology 20 (5), 491–502.

Pollard, D.D., Holzhausen, G., 1979. On the mechanical interaction between a fluid-filled fracture and the earth's surface. Tectonophysics 53, 27–57.

Stearns, D.W., 1978. Faulting and forced folding in the Rocky Mountain foreland. Geological Society of America Memoir, 151, 1–38.

Suppe, J., 1985. Principles of Structural Geology. Prentice-Hall, Englewood Cliffs, NJ, 537pp.

Tada, H., Paris, P.C., Irwin, G.R., 1985. The Stress Analysis of Cracks Handbook. Paris Productions, St. Louis, MI.

Timoshenko, S., Gooder, J.N., 1951. Theory of Elasticity. McGraw-Hill, New York.

Zehnder, A.T., Allmendinger, R.W., 2000. Velocity field for the trishear model. Journal of Structural Geology 22, 1009–1014.